JCI insight

RESEARCH ARTICLE

SorCS2-mediated NR2A trafficking regulates motor deficits in Huntington's disease

Qian Ma,[1] Jianmin Yang,[2,3] Teresa A. Milner,[4,5] Jean-Paul G. Vonsattel,[6] Mary Ellen Palko,[7] Lino Tessarollo,[7] and Barbara L. Hempstead[2,4]

[1]Graduate Program of Neuroscience, [2]Department of Medicine, Weill Cornell Medicine, New York, New York, USA. [3]Key Laboratory of Shaanxi Province for Craniofacial Precision Medicine Research, College of Stomatology, Xi'an Jiaotong University, Xi'an, People's Republic of China. [4]Feil Family Brain and Mind Research Institute, Weill Cornell Medicine, New York, New York, USA. [5]Laboratory of Neuroendocrinology, The Rockefeller University, New York, New York, USA. [6]The New York Brain Bank/Taub Institute Columbia University, Children's Hospital, New York, New York, USA. [7]Mouse Cancer Genetics Program, Center for Cancer Research, NCI, Frederick, Maryland, USA.

Motor dysfunction is a prominent and disabling feature of Huntington's disease (HD), but the molecular mechanisms that dictate its onset and progression are unknown. The N-methyl-D-aspartate receptor 2A (NR2A) subunit regulates motor skill development and synaptic plasticity in medium spiny neurons (MSNs) of the striatum, cells that are most severely impacted by HD. Here, we document reduced NR2A receptor subunits on the dendritic membranes and at the synapses of MSNs in zQ175 mice that model HD. We identify that SorCS2, a vacuolar protein sorting 10 protein–domain (VPS10P-domain) receptor, interacts with VPS35, a core component of retromer, thereby regulating surface trafficking of NR2A in MSNs. In the zQ175 striatum, SorCS2 is markedly decreased in an age- and allele-dependent manner. Notably, SorCS2 selectively interacts with mutant huntingtin (mtHTT), but not WT huntingtin (wtHTT), and is mislocalized to perinuclear clusters in striatal neurons of human HD patients and zQ175 mice. Genetic deficiency of SorCS2 accelerates the onset and exacerbates the motor coordination deficit of zQ175 mice. Together, our results identify SorCS2 as an interacting protein of mtHTT and demonstrate that impaired SorCS2-mediated NR2A subunit trafficking to dendritic surface of MSNs is, to our knowledge, a novel mechanism contributing to motor coordination deficits of HD.

Introduction

Huntington's disease (HD) is a progressive neurodegenerative disorder caused by an expansion of CAG trinucleotide repeats (>35 repeats) in exon I of the *interesting transcript 15* (*IT15*) gene, which encodes the huntingtin (HTT) protein (1). The CAG triplets result in an elongated stretch of glutamines in the N-terminal portion of HTT. Motor disorders — including involuntary movements, muscle rigidity (2), impaired balance and coordination (3–6), and impaired motor skill learning (7, 8) — are a prominent feature of behavioral symptoms of HD. The disease usually manifests in midlife and is fatal 10–15 years from the onset of symptoms (9, 10). However, the molecular mechanisms underlying the motor dysfunction in HD remain incompletely understood.

The striatum, the brain region that degenerates most significantly in HD (11), plays an important role in controlling voluntary behavior and motor skill acquisition (12). Medium spiny neurons (MSNs) are the projection neurons within the striatum and comprise about 96% of the total striatal neurons (13). All MSNs express NMDA glutamate receptors (NMDARs) (14) and receive excitatory glutamatergic inputs from the cortex and the thalamus (15). In the adult striatum, NMDARs form as heterotetramers that are typically constituted of 2 NR1 subunits and 2 NR2 (NR2A and/or NR2B) subunits (16). NMDAR subunits play a crucial role in regulating striatum-mediated motor function. For example, mice lacking the essential NR1 subunit specifically in the striatum have disrupted motor learning and deficits in long-term synaptic plasticity (17, 18). In addition, NR2 subunits control the electrophysiological properties of NMDARs (19). In HD patients, genetic variations of NR2 subunits have been shown to modify the age of onset of motor

Conflict of interest: The authors have declared that no conflict of interest exists.

Submitted: June 15, 2016
Accepted: March 30, 2017
Published: May 4, 2017

Reference information:
JCI Insight. 2017;2(9):e88995. https://doi.org/10.1172/jci.insight.88995.

symptoms in HD patients (20–22), and the function of NR2 subunits is also significantly reduced in the striatum from HD brains compared with normal brains, as assessed by glutamate bindings (23, 24). Furthermore, NR2A and NR2B subunits play distinct roles in striatum-mediated motor functions. Unilateral skill training induces an increase of NR2A and decrease of NR2B in the ipsilateral striatum in rats (25). Consistent with this, selective pharmacological inhibition of striatal NR2A subunit activity, but not NR2B subunit activity, interferes with rotarod performance in mice (26). Collectively, these observations suggest that diminished NR2A subunit activity in the striatum may contribute to the impairment of motor skill learning in HD.

The molecular mechanisms that regulate the intracellular trafficking of NR2 subunits are largely unknown. VPS10P-domain receptors consist of a related family of proteins (including SorLA, sortilin, SorCS1, SorCS2, and SorCS3), which regulate neuronal viability and function (27). Recent studies have suggested that the SorCS (sortilin-related CNS expressed) subgroup of VPS10P receptor family may play a key role in glutamate receptor trafficking to the cell surface and impact synaptic plasticity in the adult brain (28, 29).

To assess whether trafficking and surface presentation of NR2A subunits is perturbed in HD MSNs, we utilized the zQ175 mouse model of HD, which includes ~188 CAG repeats contained within a chimeric human/mouse exon 1 of murine *HTT* gene (30) and has been well established as a robust mouse model to study molecular mechanisms and therapeutic interventions of HD (30–34). Here, using quantitative analysis of immuno-electron microscopy (EM), we demonstrate that in symptomatic zQ175 mice, NR2A labeling is significantly reduced on the dendritic plasma membrane and at the synapses of MSNs and it becomes more restricted to the cytoplasm of MSNs. We identified SorCS2 as a sorting receptor that interacts with NR2A and regulates the surface expression of NR2A in MSNs dendrites. Importantly, we observed that SorCS2 interacts with mutant HTT (mtHTT) but not normal HTT, resulting in the mislocalization of SorCS2 in striatal neurons of both human HD patients and zQ175 mice, as well as a reduction of SorCS2 in the zQ175 striatum. Furthermore, SorCS2 haploinsufficiency accelerates the onset and exacerbates the motor coordination deficit of zQ175 mice. Taken together, our results identified SorCS2 as a sorting receptor that regulates NMDAR trafficking and suggest that impaired SorCS2-mediated surface trafficking of NR2A in MSNs is a novel molecular mechanism that contributes to the motor skill deficits in HD.

Results

Decreased plasma membrane expression of NR2A on the dendrites of MSNs of zQ175 mice. The relative content of NR2A subunits of NMDA receptors (NMDARs) plays a key role in motor skill performance (25, 26) and is genetically associated with HD age of onset (20–22). Therefore, we tested whether NR2A subunit trafficking and surface expression are altered in symptomatic zQ175 mice. Using double-labeling immuno-EM, we identified dendrites (Figure 1A) and dendritic spines (Figure 1B) of MSNs by their expression of dopamine and cAMP-regulated phosphoprotein-32 (Darpp-32) and located NR2A in these compartments with silver-intensified immunogold particle (NR2A-SIG). Ultrastructural analysis reveals that there is significant reduction of NR2A-SIG present on the plasma membrane of MSN dendrites in zQ175 homozygous mice compared with WT mice at the age of 12 months (Figure 1C), at which time zQ175 homozygous mice exhibit severe motor coordination deficits (30). In contrast, density of NR2A-SIG within the cytoplasm of the dendrites of MSNs is markedly increased in zQ175 homozygous mice, with similar total density of dendritic NR2A-SIG compared with WT mice (Figure 1D). We also found that the percentage of NR2A-SIG–labeled MSN dendritic spines was not significantly different between genotypes (Figure 1E). However, less NR2A-SIG is present at the synapses and more retained in the cytoplasm of MSN dendritic spines in the zQ175 homozygous mice compared with WT mice at the age of 12 months (Figure 1F). These results indicate that, in the symptomatic stage of zQ175 mice, significantly fewer NR2A-containing NMDARs are trafficked to the dendritic surface and the synaptic region of MSNs. Since NR2A subunit plays an important role in synaptic plasticity and motor skill learning, deficient NR2A subunit surface trafficking in MSNs may underlie impaired motor coordination observed in the zQ175 mouse model of HD.

SorCS2 interacts with NR2A and regulates its surface expression in dendrites of MSNs. Recent studies suggest that SorCS1 and SorCS3 are both involved in glutamate receptor trafficking (28, 29). Based on extensive homology among SorCS receptors in the ectodomain region, we posited that SorCS2 might have similar functions in trafficking of transmembrane receptors. To test this hypothesis, we first assessed whether SorCS2 is expressed in the adult mouse striatum utilizing immunofluorescence staining and observed specific immunodetection

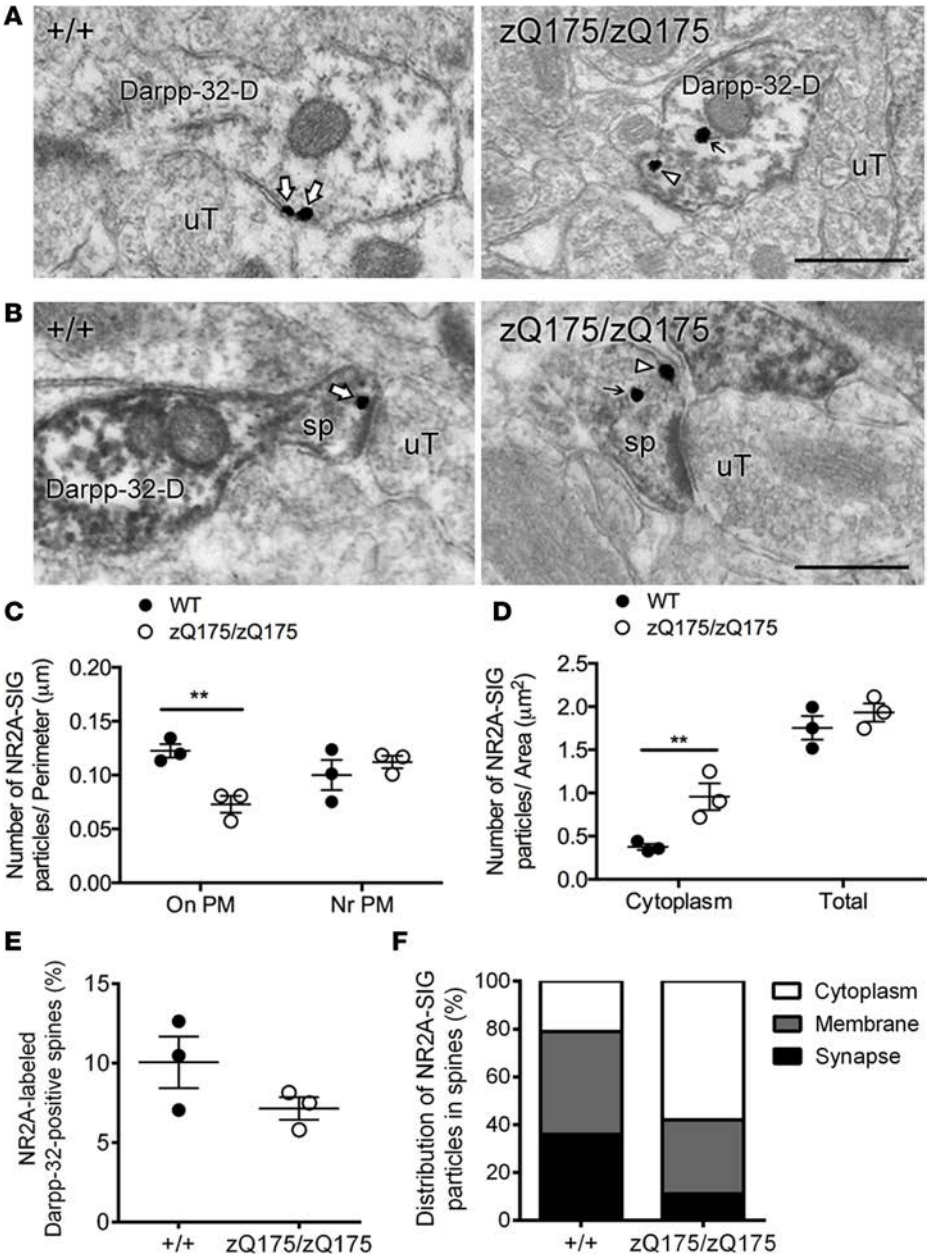

Figure 1. NR2A density on plasma membrane (PM) and synapses of Darpp-32–labeled MSN dendrites is significantly decreased in symptomatic zQ175 homozygous mice. (**A**) Representative electron micrographs of Darpp-32–containing dendrites (Darpp-32-D) showing that NR2A silver-intensified immunogold (NR2A-SIG) particles were less frequently found on PM of medium spiny neurons in zQ175 homozygous mice (right panel) than WT mice (left panel) at the age of 12 months. Unlabeled terminals (uT) are shown for comparison. White arrows, NR2A-SIG particle on PM; white arrowhead, NR2A-SIG particle near PM; arrow, NR2A-SIG particle in the cytoplasm. Scale bar: 500 nm. (**B**) Representative electron micrographs showing that NR2A-SIG particles associate more frequently with synapses in the Darpp-32–labeled spines (sp) of WT mice (left panel) than those of zQ175 homozygous mice (right panel) at the age of 12 months. The Darpp-32–containing spine in the left panel emanates from the shaft of a Darpp-32–labeled dendrite. Unlabeled terminals (uT) are shown for comparison. White arrows, NR2A-SIG particle on or near the synapses; white arrowhead, NR2A-SIG particle on or near dendritic plasma membrane; arrow, NR2A-SIG particle in the cytoplasm. Scale bar: 500 nm. (**C**) Ultrastructural analysis showed that density of NR2A-SIG particles on PM of MSN dendrites is reduced significantly in zQ175 homozygous mice compared with WT. No difference was observed in density of NR2A-SIG particles near PM (nr PM) of MSN dendrites. (**D**) zQ175 homozygous animals show significantly greater density of NR2A-SIG particles in the cytoplasm of MSN dendrites than WT. Total density of NR2A-SIG within MSN dendrites is similar between genotypes. (**E**) Graph showing that the percentages of Darpp-32–labeled spines that contain NR2A-SIG particles are not statistically different between WT and zQ175 homozygous mice. Fifty spines of each animal were analyzed. (**F**) Contingency plot showing the relative distribution of NR2A-SIG particles in Darpp-32–labeled spines. WT mice (total of 28 dual-labeled spines) have more NR2A-SIG particles associated with synapses and less retained within the cytoplasm compared with zQ175 homozygous mice (total of 18 dual-labeled spines). Number of NR2A-SIG particles associated with nonsynaptic membrane is similar between genotypes. (**C–F**) n = 3 animals/genotype; $^{**}P < 0.01$; unpaired 2-tailed student t test. Data are presented as mean ± SEM in dot plots.

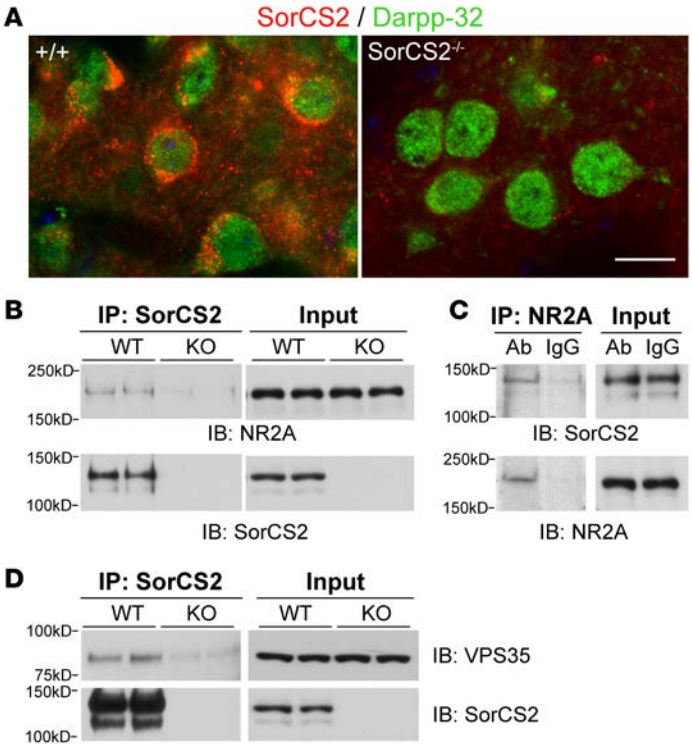

Figure 2. SorCS2 is expressed in medium spiny neurons of mouse striatum and interacts with NR2A in striatal lysates. (**A**) Immunofluorescence staining in adult mouse striatum using antibodies against SorCS2 (red) and Darpp-32 (green), a marker for medium spiny neurons. Immunolabeling of SorCS2 exhibits punctate staining pattern in the soma of Darpp-3–labeled neurons in WT striatum (left panel). SorCS2 immunoreactivity is absent in *SorCS2*$^{-/-}$ striatum (right panel). n = 3 animals/genotype; scale bar: 10 μm. (**B**) Co-IP of NR2A with SorCS2 in adult mouse striatal lysate using antibodies against SorCS2. KO, *SorCS2*$^{-/-}$. (**C**) Co-IP of SorCS2 with NR2A in adult mouse striatal lysate using antibodies against NR2A. Ab, rabbit antibody against NR2A used in IP; IgG, rabbit IgG used in IP as a negative control. (**D**) Co-IP of VPS35 with SorCS2 in adult WT mouse striatal lysate using antibody against SorCS2. The same experiments were also run in parallel using *SorCS2*$^{-/-}$ (KO) tissue as a negative control for antibody specificity. (**B–D**) Three independent experiments were conducted.

in MSNs (Figure 2A). Next we performed co-IP from striatal tissue lysates using an antibody specific for SorCS2 and probed for NR2A. We observed that NR2A could be coprecipitated with SorCS2 from WT striatal tissue but not from striatal tissue with deficient SorCS2 expression (Figure 2B). Coprecipitation of SorCS2 was also observed in a similar experiment using a specific antibody against NR2A (Figure 2C). These data demonstrate specific interaction of the NR2A subunit with SorCS2 in WT striatum.

To determine whether SorCS2 is involved in NR2A subunit trafficking, we utilized double-labeling immuno-EM to quantitate the distribution of NR2A immunoreactivity in the dendrites (Figure 3A) and dendritic spines (Figure 3B) of MSNs in WT and *SorCS2*$^{-/-}$ mice. Similar to zQ175 mice, NR2A-SIG on the plasma membrane of MSN dendrites in *SorCS2*$^{-/-}$ mice is decreased significantly compared with WT mice at the age of 12 months (Figure 3C). In contrast, cytoplasmic NR2A-SIG in the MSN dendrites is significantly increased in *SorCS2*$^{-/-}$ mice, although the total density of dendritic NR2A-SIG in both genotypes is comparable (Figure 3D). Moreover, we found that SorCS2 deficiency did not alter the percentage of NR2A-SIG–labeled MSN dendritic spines (Figure 3E), but there were fewer NR2A-SIG particles labeled at the synapses and more were retained in the cytoplasm of MSN dendritic spines in *SorCS2*$^{-/-}$ mice compared with WT mice at the age of 12 months (Figure 3F). These results demonstrate that deficiency of SorCS2 leads to significantly fewer NR2A-containing NMDARs trafficked to the dendritic and the synaptic surface of MSNs. From these observations, we conclude that SorCS2 is a key regulator of NR2A dendritic trafficking in MSNs.

To further dissect the underlying molecular mechanism of SorCS2-mediated NR2A trafficking and its impairment in HD, we specifically chose to evaluate components of the retromer complex, which have been identified as interacting partners of HTT protein (35). We identify that VPS35, a core component of retromer complex, interacts with SorCS2 in WT adult striatal lysate (Figure 2D). Importantly, VPS35 is also essential for the local recycling of NMDARs back to dendritic surface (36). Thus, recycling of NR2A by retromer and its interaction with SorCS2 provide a new mechanism for SorCS2-mediated NR2A trafficking, which might be impaired in HD striatal neurons.

We have also mapped the regions of SorCS2 that are required for coprecipitation of NR2A. In this structure-function approach using SorCS2 mutagenesis, we observe that the ectodomain of SorCS2 is required, whereas the intracellular domain is dispensable in a reconstituted cell assay system (Supplemental Figure 6; supplemental material available online with this article; https://doi.org/10.1172/jci.insight.88995DS1). This is consistent with prior studies of the related SorCS1 receptor, which interacts with its ligand neurexin through the SorCS1 ectodomain (28).

Reduction of SorCS2 in the striatum of HD mouse models. To evaluate whether mtHTT affects the levels of expression of SorCS2 in a mouse model of HD, we first performed Western blot analysis using striatal lysates of symptomatic zQ175 mice (12 months of age). We observed a 20.8% ± 4.5% (P = 0.0214) and

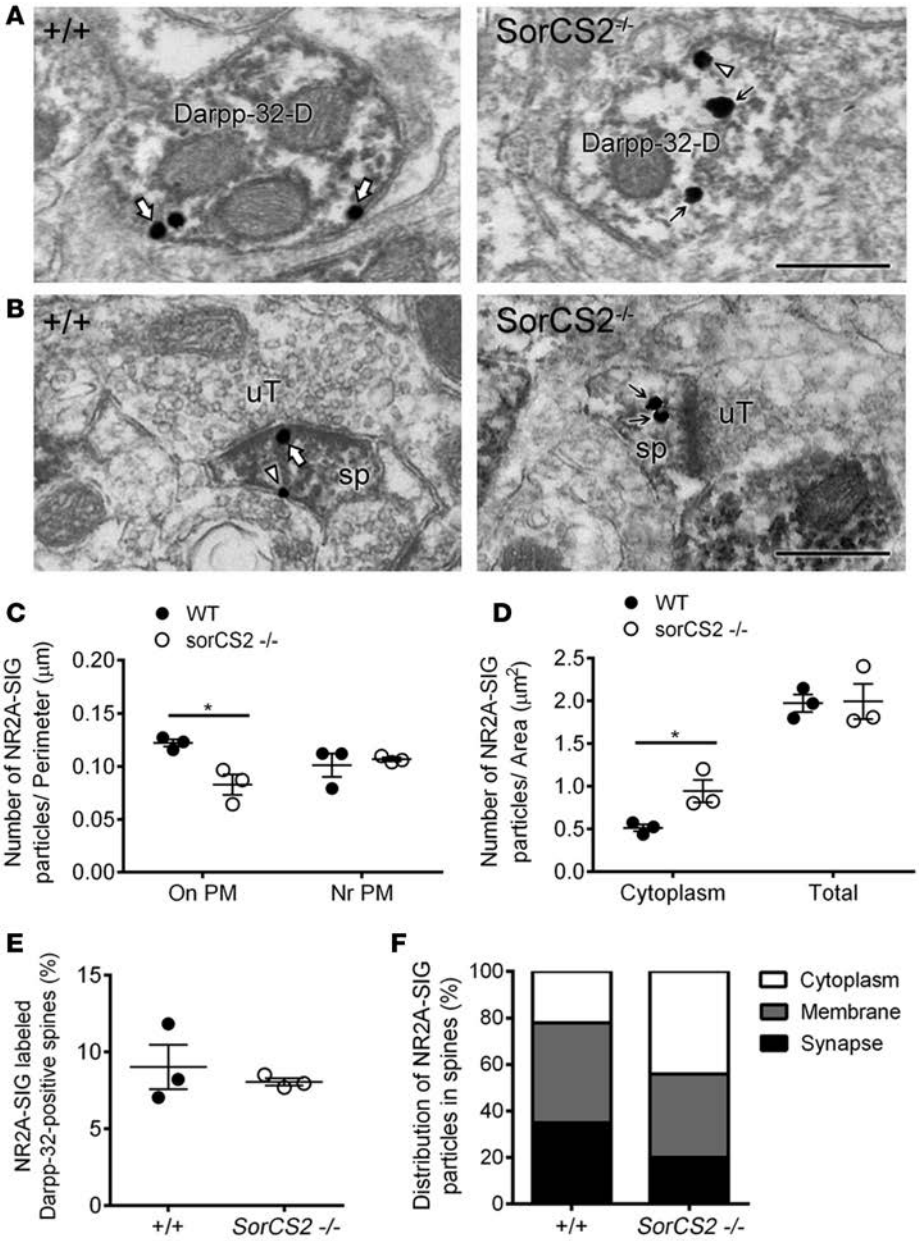

Figure 3. NR2A density on plasma membrane (PM) and synapses of Darpp-32–labeled MSN dendrites is significantly decreased in SorCS2-deficient mice. (**A**) Representative electron micrographs of Darpp-32–containing dendrites (Darpp-32-D) showing that NR2A silver-intensified immunogold (NR2A-SIG) particles are less frequently found on PM of medium spiny neurons in *SorCS2*$^{-/-}$ mice (right panel) than WT mice (left panel) at the age of 12 months. White arrows, NR2A-SIG particle on PM; white arrowhead, NR2A-SIG particle near PM; arrows, NR2A-SIG particle in the cytoplasm. Scale bar: 500 nm. (**B**) Representative electron micrographs showing that NR2A-SIG particles associate more frequently with synapses in the Darpp-32–labeled spines (sp) of WT mice (left panel) than those of *SorCS2*$^{-/-}$ homozygous mice (right panel) at the age of 12 months. Unlabeled terminals (uT) are shown for comparison. White arrow, NR2A-SIG particle on or near the synapses; white arrowhead, NR2A-SIG particle on or near dendritic plasma membrane; arrows, NR2A-SIG particle in the cytoplasm. Scale bar: 500 nm. (**C**) Ultrastructural analysis shows that density of NR2A-SIG particles on PM of MSN dendrites is reduced significantly in *SorCS2*$^{-/-}$ mice compared with WT. No difference is observed in density of NR2A-SIG particles near PM (nr PM) of MSN dendrites. (**D**) *SorCS2*$^{-/-}$ animals show significantly greater density of NR2A-SIG particles in the cytoplasm of MSN dendrites than WT. Total density of NR2A-SIG within MSN dendrites is similar between genotypes. (**E**) Graph showing that the percentages of Darpp-32–labeled spines that contain NR2A-SIG particles are not statistically different between WT and *SorCS2*$^{-/-}$ mice. Fifty spines of each animal were analyzed. (**F**) Contingency plot showing the relative distribution of NR2A-SIG particles in Darpp-32–labeled spines. WT mice (total of 23 dual-labeled spines) have more NR2A-SIG particles associated with synapses and less retained within the cytoplasm compared with *SorCS2*$^{-/-}$ mice (total of 24 dual-labeled spines). Number of NR2A-SIG particles associated with nonsynaptic membrane is similar between genotypes. (**C–F**) n = 3 animals/genotype; *$P < 0.05$; unpaired 2-tailed student t test. Data are presented as mean ± SEM in dot plots.

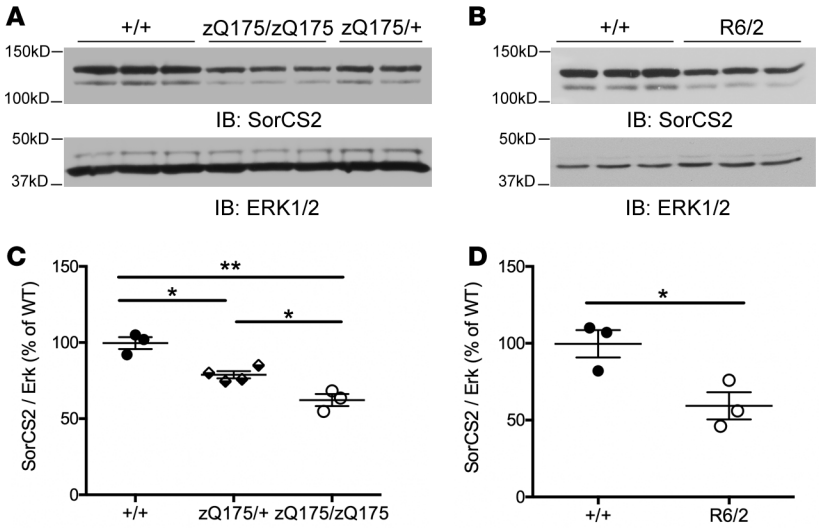

Figure 4. SorCS2 level decreases significantly in the striatum of symptomatic zQ175 mice and R6/2 mice. (**A** and **C**) Western blot analysis showing that SorCS2 protein level is significantly reduced in an allele-dependent manner in the striatal lysate of zQ175 heterozygous and homozygous animals compared with WT at the age of 12 months. n = 3–4 animals/genotype; $^*P < 0.05$; $^{**}P < 0.01$; one-way ANOVA followed by Bonferroni post hoc test. (**B** and **D**) Western blot analysis showing that SorCS2 protein level also decreases significantly in the striatal lysate of R6/2 mice (13-week-old) compared with WT littermates. n = 3 animals/genotype; $^*P < 0.05$; unpaired 2-tailed student t test. Data are presented as mean ± SEM.

37.5% ± 7.6% (P = 0.0025) reduction of SorCS2 total protein levels in the striatum of zQ175 heterozygous and homozygous animals, respectively, as compared with WT littermate controls (Figure 4, A and C). This reduction is allele dependent, given that zQ175 homozygous mice have significantly lower striatal SorCS2 (21.1% ± 3.6%) than zQ175 heterozygous mice (P = 0.0341) (Figure 4, A and C).

To confirm that this reduction in striatal SorCS2 is not specific to a single HD mouse model, we performed Western blot analysis using striatal lysates from the well-characterized R6/2 HD mouse line (37) at the age of 13 weeks of age, a symptomatic stage. Again, we observed a significant decrease in SorCS2 protein levels (39.1% ± 7.5%) in the R6/2 striatum compared with WT littermate controls (P = 0.0322) (Figure 4, B and D).

The reduction of SorCS2 protein is both age dependent and region dependent, as we observed no decrease of SorCS2 in the zQ175 striatum at 2 months of age, a time when mice are presymptomatic (Supplemental Figure 1, A and B), but we observed a significant decrease of SorCS2 in the striatal lysate of zQ175 homozygous mice at the age of 6 months (Supplemental Figure 1, C and D). Importantly, this age-related decline of SorCS2 protein level reflects a reduction of *Sorcs2* gene transcription in the striatum of 12-month-old zQ175 homozygous mice (Supplemental Figure 3). In addition, there is no significant difference of SorCS2 protein levels in many other brain regions of 12-month-old zQ175 mice or 13-week-old R6/2 mice as compared with WT littermates, including the sensorimotor cortex, the hippocampus, and the cerebellum (Supplemental Figure 2 and 4).

Collectively, these results demonstrate that SorCS2 protein levels are significantly reduced in an age- and allele-dependent manner in the mouse HD striatum. Since SorCS2 expression regulates appropriate localization of NR2A to the plasma membrane, and SorCS2-deficient animals exhibit a reduction of NR2A subunit on the dendritic surface of MSNs, the reduction in SorCS2 as a consequence of mtHTT expression may lead to the loss of NR2A on the membrane of MSNs dendrites, which in turn could contribute to the motor deficits manifested in the zQ175 mouse model of HD.

SorCS2 binds to mtHTT and is mislocalized in human HD patients and mouse models. It has been well established that HTT interacts with many proteins that play roles in intracellular trafficking and that mtHTT interacts with distinct proteins as compared with wtHTT (wtHTT) (35, 38–41). To examine whether HTT proteins interact with SorCS2 and whether SorCS2 selectively interacts with wtHTT or mtHTT, we performed co-IP studies using mouse striatal lysates followed by Western blot analysis. Notably, mtHTT — but not wtHTT — coprecipitates with SorCS2 in the striatal lysate of zQ175 heterozygous mice at the ages of 1 month (presymptomatic stage) and 12 months (symptomatic stage) (Figure 5A).

Whereas wtHTT is diffusely detected throughout the cytoplasm of human striatal neurons, mtHTT is differentially localized at a subcellular level (i.e., with a more frequent punctate distribution within the cytoplasm and in the perinuclear region, and reduced in neuritic processes), as compared with wtHTT in human striatal neurons (42). Thus, we hypothesized that SorCS2 might also exhibit altered subcellular distribution due to its selective interaction with mtHTT but not wtHTT. To test this, we examined the

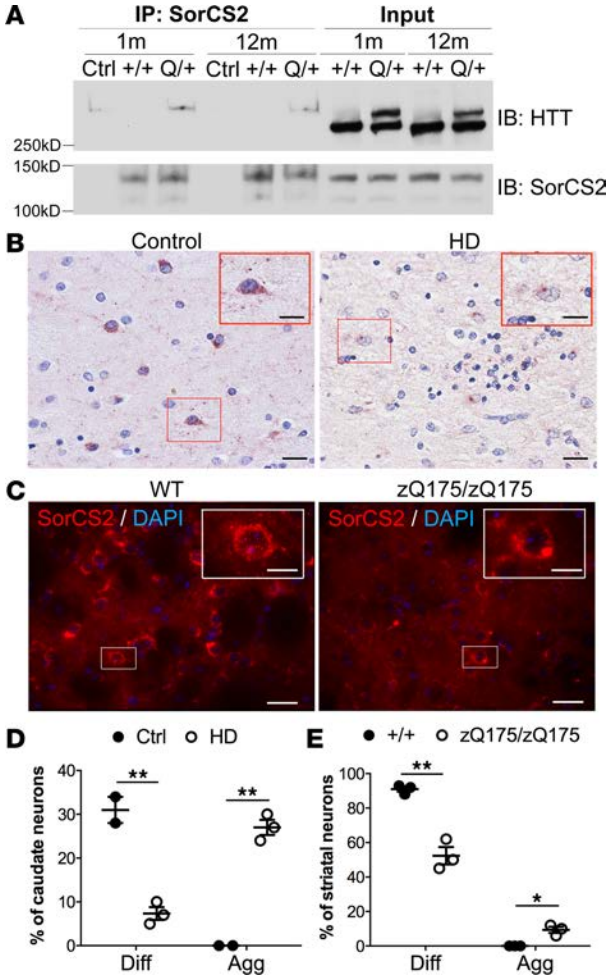

Figure 5. SorCS2 interacts with mutant huntingtin and is mislocalized in human HD caudate and mouse HD striatum. (**A**) Co-IP of mutant huntingtin, but not WT huntingtin, with SorCS2 using anti-SorCS2 antibody and mouse striatal lysates. This protein interaction is detected in lysates of mice at 1 and 12 months of age. Three independent experiments were conducted. Ctrl, control experiment using zQ175/+ tissue but without anti-SorCS2 antibody; 1m, 1-month-old; 12m, 12-month-old; Q/+, zQ175/+ mice. (**B**) Immunohistochemical detection of SorCS2 in the caudate of grade 3 human HD patients (n = 3) and controls (n = 2). In control cases (left panel), SorCS2 is diffusely stained in the somatodendritic compartment of a subset of caudate neurons. However, in HD patients (right panel), localization of SorCS2 is mainly present in perinuclear clusters in neurons of the caudate. Scale bars: 20 μm. Pictures in the top right corners are enlarged images of neurons in the small red boxes. Scale bars of inset panels: 10 μm. (**C**) Immunofluorescence detection of SorCS2 in the striatum of WT (left panel) and zQ175 homozygous mice (right panel) at the age of 12 months. Scale bars: 20 μm. Note the reduction of SorCS2 immunoreactivity and its mislocalization to perinuclear clusters in a subset of neurons in the striatum of zQ175 homozygous mice. n = 3 animals/genotype. Pictures in the top right corners are enlarged images of neurons in the small white boxes. Scale bars of inset panels: 10 μm. (**D**) Statistical analysis of the percentage of caudate neurons in human sections that exhibit diffuse (Diff) or aggregated (Agg) staining of SorCS2. n = 3 for human grade 3 HD cases; n = 2 for human control cases; $^{**}P < 0.01$; unpaired 2-tailed student t test. Data are presented as mean ± SEM. (**E**) Statistical analysis of the percentage of striatal neurons in mouse sections that exhibit Diff or Agg staining of SorCS2. n = 3 animals/genotype; $^{*}P < 0.05$; $^{**}P < 0.01$; unpaired 2-tailed student t test. Data are presented as mean ± SEM.

localization of SorCS2 in the caudate neurons from human brain sections using immunohistochemical staining. In striatal sections from unaffected individuals, SorCS2 can be detected in a subset of neurons in the caudate and is diffusely distributed in the somatodendritic cytoplasm of these neurons (Figure 5, B and D). In sections of the neostriatum of individuals with HD, the overall intensity of SorCS2 immunoreactivity is significantly decreased as compared with unaffected controls. We also observed a profound loss of diffuse labeling of SorCS2 in the cell bodies of the medium-sized neurons that are still surviving in the degenerating human HD caudate (Figure 5, B and D). Moreover, the reaction product of SorCS2 staining in these neurons is concentrated in perinuclear clusters and diminished in the neuronal processes (Figure 5B, inset of the right panel). We next immunolocalized SorCS2 in striatal neurons from zQ175 and WT mice. An overall reduction in diffuse cytoplasmic localization of SorCS2 was also noted in zQ175 homozygous mice, as compared with WT littermate controls, as well as some punctate perinuclear staining (Figure 5, C and E). However, this concentrated SorCS2 immunoreactivity does not overlap with markers of lysosomes (Supplemental Figure 5A) or mtHTT aggregates (Supplemental Figure 5B).

Our results suggest that, in addition to the overall reduction of SorCS2 protein levels in HD striatum, an aberrant interaction between mtHTT and SorCS2 precedes disease onset. This mtHTT/SorCS2 interaction may also contribute to the motor deficits of HD by interfering with the normal SorCS2 intracellular distribution and affecting NR2A trafficking.

SorCS2 deficiency regulates the onset and severity of motor coordination in zQ175 mice. Since SorCS2-mediated NR2A surface expression is perturbed in HD (Figure 1 and 3), we next asked whether a reduction in SorCS2 levels would affect the progression of the motor phenotype in HD. To test this hypothesis, we crossed SorCS2$^{+/-}$ mice with zQ175/+ mice to obtain zQ175/+ SorCS2$^{+/-}$ animals and littermate controls. Haploinsufficiency of SorCS2 and expression of the zQ175 allele had no effects on life span within the time frame evaluated (0–10 months). We measured motor coordination of these mice using the accelerating rotarod test at the age of 2 months, 6 months, and 10 months. No significant differences in motor performance were observed between any genotypes when mice were tested at 2 months of age. However, at the age of 6 months, zQ175/+ SorCS2$^{+/-}$ mice exhibited a significant impairment of motor coordination while the performance of other genotypes remained normal (Figure 6A). At later ages (10 months of age), zQ175/+ mice exhibited poorer performance on rotarod compared with WT littermates; however, zQ175/+ SorCS2$^{+/-}$ mice had more severe motor deficits compared with zQ175/+ mice (Figure 6A). This impairment of motor coordination is not due to changes in body weight

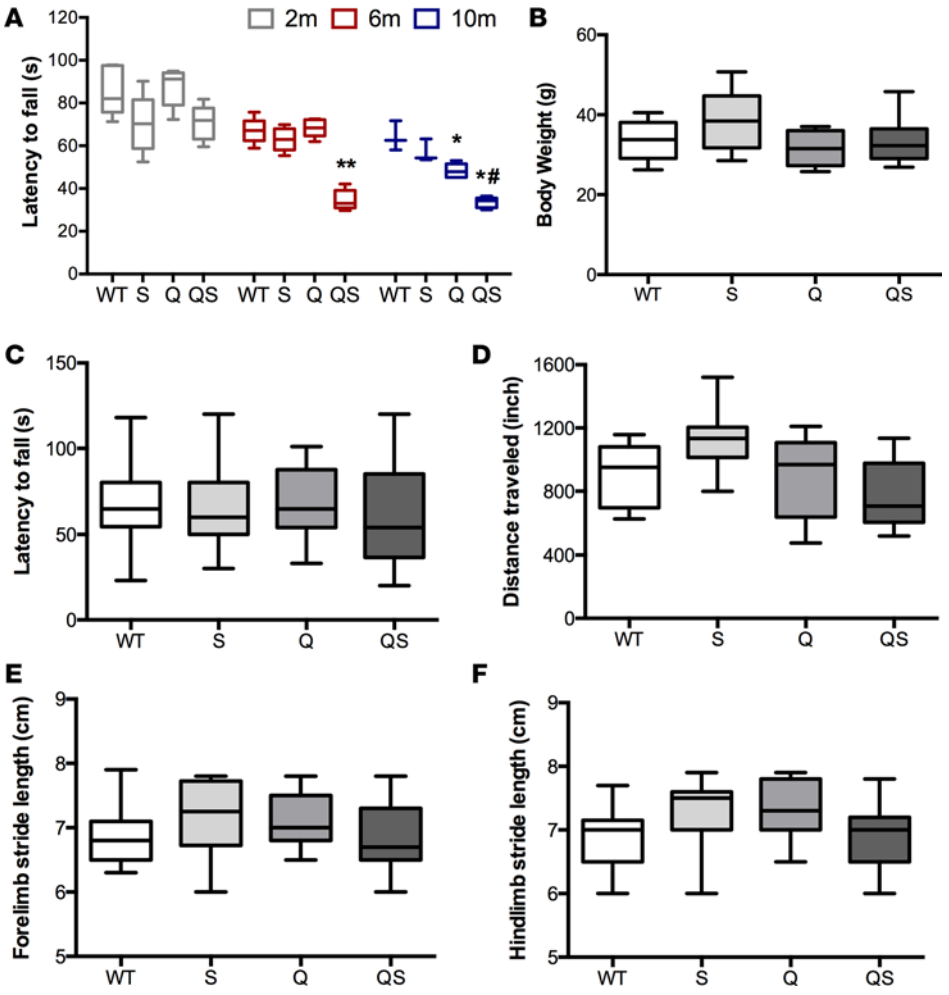

Figure 6. SorCS2 haploinsufficiency accelerates the onset of motor skill deficit of zQ175 HD mice. (**A**) Rotarod test. Mice of indicated genotypes were tested on the accelerating rotarod at 2 months (2m), 6 months (6m), and 10 months (10m). Note that zQ175/+ SorCS2$^{+/-}$ (QS) mice have significantly lower latency to fall at the age of 6 months and 10 months compared with WT, SorCS2$^{+/-}$ (S), and zQ175/+ (Q) mice. Q mice exhibit mild deficits in rotarod test at 10 months of age compared with WT littermates. (**B**) Body weight. No significant difference was observed in body weight of all the genotypes at the age of 10 months. (**C**) Inverted lid test was used to measure limb muscle strength. All the genotypes have similar latency to fall at the time point of 10 months. (**D**) Open field test. Total distance traveled was recorded to measure baseline locomotor activity of mice. All the genotypes have comparable locomotor activity at the age of 10 months. (**E** and **F**) Footprint analysis. The footprint patterns were assessed quantitatively by measurements of forelimb (**E**) and hindlimb (**F**) stride length. There was no significant difference observed in the gait patterns of all genotypes of mice at the age of 12 months. n = 8–12 mice/genotype were used in each experiment; *$P < 0.05$ (compared with WT); **$P < 0.01$ (compared with WT); $^{\#}P < 0.05$ (compared with zQ175/+); one-way ANOVA followed by Bonferroni post hoc test. In all the box and whisker plots, the boxes extend from the 25th to 75th percentile. The line in the middle of the box is plotted at the median. The whiskers go down to the minimum value and up to the maximum.

(Figure 6B), muscle strength (Figure 6C), baseline locomotor activity in the open field test (Figure 6D), or gait abnormality (Figure 6, E and F). In addition, SorCS2$^{+/-}$ mice had normal rotarod performance at all ages, as compared with WT mice, which implies that SorCS2 deficiency alone is not sufficient to cause impaired motor coordination under normal conditions. However, haploinsufficiency of SorCS2 in animals expressing mtHTT leads to acceleration of the onset and exacerbation of motor coordination deficits of zQ175 mice.

Discussion

Motor skill disability is one of the most prominent features of HD, yet the precise molecular mechanisms that lead to these deficits are not clear. Here, we identify SorCS2 as an mtHTT interacting partner that regulates targeting NR2A subunits to the plasma membrane and the synapses of striatal neurons,

and we demonstrate that impaired SorCS2-mediated striatal NR2A trafficking contributes to motor deficits in the zQ175 mouse model of HD.

NMDARs in HD pathogenesis. In HD, NMDARs have been best characterized as mediators of elevated Ca^{2+} signaling and subsequent excitotoxic damage to MSNs (39, 43–47). This prevailing excitotoxicity hypothesis is based on the early observations that the levels of NMDARs are decreased in striatal neurons of HD human patients (23) and that injection of NMDA agonist quinolinic acid into rodent striatum can recapitulate some behavioral and pathological alterations of HD (48, 49). Notably, recent studies have revealed that this susceptibility to excitotoxicity is biphasic in HD mouse models. NMDAR currents are reported to be elevated in the striatum of HD mice in early symptomatic stages, possibly due to increased NR2B-containing (43, 46) and NR3A-containing NMDARs (39) on the cell surface. In contrast, HD mice become resistant to insults of NMDA agonists in later symptomatic stages (50, 51), correlating with significantly reduced NMDA currents in the HD striatum (50). However, the molecular mechanisms underlying the decreased striatal NMDAR activity in symptomatic HD mice and its potential implications on the progression of HD symptoms have not been elucidated.

Our results documenting deficient SorCS2-mediated trafficking of NR2A to the dendritic surface and the synapses of the MSNs in the striatum of symptomatic zQ175 mice, to our knowledge, provide a novel mechanism underlying the diminished NMDAR activity and manifestation of motor symptoms in later stages of HD. Given that NMDAR is essential in defining Ca^{2+} influx and synaptic strength (52), our data supports a recent hypothesis that deficits in endomembrane recycling and Ca^{2+} homeostasis can lead to late-onset synaptic degeneration in multiple neurodegenerative disorders, including Alzheimer's disease, Parkinson's disease, amyotrophic lateral sclerosis, and HD (53). Sufficient signaling of NMDAR at the synapses is needed to keep steady-state levels of synaptic calcium–dependent kinases activities and maintain robust neuronal connections (54). For example, disruption of the CaMKII complex with NMDAR leads to persistent reduction of the synaptic strength and weakening of hippocampal synapses (52). In this regard, our finding of impaired surface presentation of synaptic NR2A in HD MSNs is in line with reduced excitatory postsynaptic currents (EPSCs) (31), deficient striatal long-term synaptic plasticity (33), and reduced spine density of MSNs (55) observed in the zQ175 mouse model at the symptomatic stage. In addition, since NR2A-containing NMDARs have been found to have protective effects on neuronal survival (56–58), insufficient synaptic NR2A signaling could increase the vulnerability of MSNs in HD and account for the direct correlation between clinical motor impairment and striatal atrophy observed in human HD patients (59, 60). Therefore, strategies to enhance the surface levels of synaptic NR2A receptor units in the HD striatum would provide new approaches to maintain proper levels of cortico-striatal synaptic activity and ameliorate motor impairment in symptomatic HD patients.

Role of SorCS2 in dendritic trafficking of NR2A subunits. Synaptic NR2 subunits of NMDARs play a pivotal role in synaptic refinement (16). Targeting an appropriate number of NR2 subunits to the postsynaptic sites at synapses is critical for normal glutamatergic neurotransmission and synaptic plasticity (61). In terms of their surface distribution and trafficking, it has been well established that interactions of NR2B subunits with membrane-associated guanylate kinases (MAGUKs), particularly SAP102, and other associated protein complexes at the postsynaptic density are required to impart their synaptic entry and retention (62, 63). However, it has been suggested that synaptic targeting of NR2A does not employ similar mechanisms as those of NR2B (63). Although some reports have shown that phosphorylation (64) and palmitoylation (65) of NR2A subunits can affect their trafficking, the sorting mechanisms that regulate transport of NR2A into the dendritic plasma membrane and synaptic localization remain elusive.

Recent studies have focused on sorting receptors, including VPS10P receptors that bind a range of ligands, from small secretable proteins such as neurotrophic factors (66, 67) to large transmembrane proteins including amyloid precursor protein (APP) (68) and Trk receptors (69). For example, sortilin regulates endosomal sorting and lysosomal degradation of brain-derived neurotrophic factors (66, 70), as well as anterograde trafficking of TrkB receptors (69, 71), while SorLA has been shown to mediate retrograde retention of APP in the trans-Golgi network (68). It has been shown that the ectodomains of VPS10P receptors are responsible for cargo binding (28, 66), whereas their intracellular domains dictate the trafficking routes and can vary considerably among different VPS10P family members (72).

Important roles of other members of the SorCS subgroup of the VPS10P receptor family in glutamate receptor trafficking have recently been described (s28, 29). SorCS1 is shown to mediate α-amino-

3-hydroxy-5-methyl-4-isoxazolepropionic acid (AMPA) receptor surface trafficking and is indispensable for synaptic long-term potentiation in the hippocampus (28), while SorCS3 is necessary for long-term synaptic depression via regulating glutamate receptor trafficking to the synapse (29). Here, we find that SorCS2 can interact with an NR2A subunit of NMDARs, which is crucial for the surface presentation of NR2A in MSN dendrites as well as its targeting to the synapses of MSNs.

Our finding that VPS35, a key component of the retromer complex, is a binding partner of SorCS2 is consistent with the literature that the retromer complex binds directly to other VPS10P family members sortilin and SorLA (73–75), utilizing aromatic motifs in the cytoplasmic tail of VPS10P sorting receptors (76). The retromer complex is emerging as a major regulator of endosomal sorting (77) and maintains surface expression of membrane proteins by retrieving cargo for recycling (78, 79) as well as preventing their lysosomal degradation (80). Importantly, it has been shown that retromer also interacts with HTT protein (35) and regulates local NMDAR recycling in dendrites (36). Loss of retromer activity can cause diminished NMDA currents (36), progressive synaptic dysfunction, and neuronal degeneration (81), which are reminiscent of the phenotypes reported in HD mouse models (31, 50, 55).

Interestingly, HAP1, the first identified HTT-associated protein, has been shown to stabilize the complex of TrkB and sortilin, another VPS10P family sorting receptor, to facilitate TrkB anterograde trafficking and prevent its lysosomal degradation. However, we observed no similar interaction of SorCS2 with HAP1 in vitro or in vivo (data not shown).

Collectively, our data suggests that SorCS2 plays a crucial role in replenishing the pool of NR2A on the dendritic and synaptic surface of MSNs by interacting with retromer and promoting NR2A recycling back to the cell surface. Future studies will be needed to delineate the trafficking routes by which SorCS2 regulates the sorting and surface delivery of NR2A in neurons in order to better understand the underlying mechanisms of SorCS2-mediated receptor trafficking at a molecular and cellular level.

VPS10P family members as interacting proteins of mtHTT. HTT protein is a scaffolding protein that regulates multiple aspects of trafficking of transmembrane receptors, including endocytosis (82), endosomal sorting (83), anterograde transport (71, 84), degradation (71, 83, 84), and recycling (85, 86). It has been shown that mtHTT can inhibit the surface expression of receptors via its interactions with trafficking proteins such as Rab11 (87) and HAP1 (71, 83, 84), proteins that prevent lysosomal degradation and promote recycling of their cargo receptors back to the cell surface (88). For example, mtHTT can bind to and interfere with the nucleotide exchange activity of Rab11, a small GTPase that functions at recycling endosomes, and impede the membrane recycling of its cargo such as transferrin receptor (89), solute carrier EAAC1 (87), and glucose transporter 3 (90). mtHTT also binds more tightly to HAP1 compared with wtHTT, thereby disrupting the synaptic targeting of $GABA_A$ receptor (83) and the anterograde trafficking of TrkA receptor (84).

Although VPS10P family members have been previously linked to several neurodegenerative diseases (27), little is known about whether mtHTT interferes with the function of VPS10P-regulated trafficking and its implication in HD pathogenesis. Here, we identify SorCS2 as a trafficking regulator interacting selectively with mtHTT but not wtHTT. Our observations of mislocalization of SorCS2 and the defective trafficking of its cargo NMDAR in HD striatal neurons suggest that the differential interaction of SorCS2 with HTT proteins, which can occur at both early and late stages of the disease, is one of the pathogenic mechanisms that contributes to the HD motor phenotype. Further studies will be required to determine how key components within the SorCS2/mtHTT complex are mechanistically affected in HD striatal neurons at a molecular level.

In conclusion, our results provide a new mechanism by which mtHTT leads to dysfunction of striatal neurons and manifestation of motor deficits in HD via perturbation of protein trafficking processes, specifically interfering with the role of SorCS2 to modulate the synaptic expression of NMDAR. Identification of other key cargos whose trafficking is disrupted by the anomalous binding of mtHTT to SorCS2 will facilitate our understanding of the pathophysiology of HD and open up new avenues to develop treatments for this neurodegenerative disorder.

Methods

Supplemental Methods are available online with this article.

Mouse strains. The zQ175-knockin mouse line was supplied from The Jackson Laboratory (stock no. 370437) with CAG repeats ranging from 170–200. R6/2 breeding females (C57Bl6 females with

transplanted ovaries from R6/2 females with 200–250 CAG repeats) were purchased from The Jackson Laboratory (stock no. 371097) and were bred with C57Bl6 males to generate R6/2 transgenic mice and their WT littermates. SorCS2-KO mice were previously generated (J. Yang, unpublished observations). Briefly, the *sorCS2* gene targeted mice were generated by deleting exon 2 of the gene, using a targeting vector for *sorCS2* purchased from the European Conditional Mouse Mutagenesis Program (EUCOMM), with loxP sites flanking exon 2 of the *sorCS2* gene. Following blastocyst reaggregation with positive ES clones, animals were obtained with the disrupted allele as assessed by Southern blot analysis. SorCS2-deficient mice were generated by crossing with EIIa-Cre expressing mice (The Jackson Laboratory), and mice were backcrossed to C57/Bl6 for more than 9 generations. zQ175/+ mice were then bred with SorCS2$^{+/-}$ mice to generate zQ175/+ SorCS2$^{+/-}$ mice, zQ175/+ mice, SorCS2$^{+/-}$ mice, and WT littermates. Only male mice were used studies.

Immunofluorescence staining and analysis. Mice were injected with sodium pentobarbital (150 mg/kg, i.p.) and transcardially perfused with cold phosphate-buffered saline (PBS, pH 7.4), followed by 4% paraformaldehyde (PFA) in PBS. Brains were post-fixed in 4% PFA overnight at 4°C and then cryoprotected with 30% sucrose in PBS. Free-floating coronal brain sections (30 μm) were prepared on a freezing microtome. For immunofluorescence detection, brain sections were incubated in blocking buffer (5% normal donkey serum (Jackson ImmunoResearch) and 0.3% Triton-X 100 (Sigma) in PBS, pH 7.4) and avidin/biotin blocking kit (Vector Laboratories, SP-2001) at room temperature, and then incubated with primary antibodies in blocking buffer for 18 hours at 4°C. The following primary antibodies were used: sheep anti-SorCS2 (1:1,000, R&D Systems, AF4237), mouse anti–Darpp-32 (gift from Hugh C. Hemmings, Weill Cornell Medicine, New York, NY, USA), mouse anti–mutant HTT (1:100, Millipore, EM48), rabbit anti-GFAP (DAKO, Z0334, 1:1,000), and rat anti-LAMP1 (BD Biosciences, catalog 553792, 1:500). The secondary antibodies used were biotinylated donkey anti–sheep IgG (1:400, Jackson ImmunoResearch, catalog 713-065-147) and donkey anti–mouse, –rabbit, or –rat Alexa 488 (1:1,000; Invitrogen; catalogs R37114, A21206, A21208, respectively). Cy3-conjugated streptavidin (1:1,000, Jackson ImmunoResearch, catalog 016-160-084) was used to visualize biotinylated secondary antibodies. Three animals per genotype were analyzed for each experiment. Immunofluorescence images were examined on Zeiss Axio Observer.Z1 inverted microscope and captured using the same exposure time/channel/experiment by AxioCam MRC camera between different genotypes. Quantitative analyses (mean pixel intensity measurement or cell count per field) were performed using Image J v1.33 software by Wayne Rasband (NIH).

Co-IP and Western blot analysis. Dissected tissues were minced and lysed in lysis buffer (1% NP-40, 1% Triton X-100, 1 mM PMSF, 10% glycerol and protease inhibitor cocktail (Sigma-Aldrich) in Tris-buffered saline) for 30 minutes on ice. Lysates were further titrated using a 30-g needle, and supernatants were collected following centrifugation at 16,000 *g* for 5 minutes. Cleared lysates were then resolved by SDS-PAGE. For IP, samples were first precleared using protein G-Sepharose beads (Invitrogen, catalog 101241), and the supernatant was then incubated with sheep anti-SorCS2 antibody (R&D Systems, catalog AF4237) for 18 hours at 4°C. Similar experiments were performed for NR2A co-IP using protein A-Sepharose beads (Sigma-Aldrich, catalog P9424) and rabbit anti-NR2A antibody (Thermo Fisher Scientific, catalog OPA1-04021). Sepharose beads were then added to the supernatant for 2 hours at 4°C, and immunoprecipitates were collected by centrifugation for 5 minutes at 2,300 *g*. Beads were washed 3 times in lysis buffer, and immune-complexes were resolved by SDS-PAGE. Following transfer, Western blots were blocked and incubated with primary antibodies, followed by labeling with HRP-conjugated secondary antibodies, and were developed with the ECL kit (Amersham, catalog RPN2106). The following primary antibodies were used: rabbit anti-ERK1/2 (1:3,000, Cell Signaling Technology, catalog 9102S), sheep anti-SorCS2 (1:1,000, R&D Systems, catalog AF4237), mouse anti-HTT (1:1,000, Millipore, catalog MAB2166), rabbit anti-NR2A (1:2,000, Thermo Fisher Scientific, catalog PA5-35377), and rabbit anti-VPS35 (1:1,000, Abcam, catalog ab157220). Three animals per genotype were used for each experiment. In Western blot densitometry analysis, values were normalized by loading control protein levels and then averaged to compare with WT mice.

Electron microscopy. Sections were processed for electron microscopy as previously described (91). Briefly, 12-month-old WT, zQ175 homozygous mice, or *SorCS2*$^{-/-}$ mice were overdosed with sodium pentobarbital (150 mg/kg, i.p.) and perfused transcardially with 2% heparin-saline followed by 30 ml, 3.75% acrolein, and 2% PFA in 0.1 M phosphate buffer (PB; pH 7.4). The brains were removed from

the skull, post-fixed in 2% acrolein and 2% PFA in PB for 30 minutes, and then placed in PB. Coronal sections through the brains were cut (40-μm thick) using Vibratome (Leica Microsystems) and stored in cryoprotectant at –20°C until use.

For NR2A/Darpp-32 dual-immunolabeling, striatal sections (n = 3 animals per genotype, 2 sections per animal) were rinsed in PB to remove cryoprotectant and then incubated in 1% sodium borohydride in PB for 30 minutes to remove active aldehydes. Sections were then washed in 8–10 changes of PB until all the gaseous bubbles disappeared and then placed in 0.1 M Tris-buffered saline (TS), pH 7.6. Sections were then incubated sequentially in: (i) 0.5% BSA in TS (30 min); (ii) primary antibodies (rabbit anti-NR2A (1:50, Thermo Fisher Scientific, catalog PA5-35377) and mouse anti–Darpp-32 (1:1,000, gift from Hugh C. Hemmings) in 0.1% BSA in TS for 1 day at room temperature (~23°C), followed by 4 days cold (~4°C); (iii) 1:400 of biotinylated anti-goat IgG (Jackson ImmunoResearch, catalog 705-065-147), 30 minutes ; (iv) 1:100 peroxidase-avidin complex (Vectastain Elite Kit, Vector Laboratories, catalog PK-6100), 30 minutes; and (v) DAB (Sigma-Aldrich) and H_2O_2in TS, 3 minutes. All incubations were separated by washes in TS. For immunogold detection of NR2A, the DAB-reacted sections were rinsed in 0.01 M PBS (pH 7.4), incubated in blocking buffer (0.8% BSA, 0.2% gelatin, 0.02% BSAc in 0.02 M PBS) for 30 minutes, and placed overnight in a 1:50 dilution of donkey anti–rabbit IgG with bound 10-nm colloidal gold (Electron Microscopy Sciences, catalog 25704) diluted in blocking buffer. The gold particles were fixed to the tissue in 2% gluteraldehyde in 0.01 M PBS and rinsed in PBS followed by 0.2 M sodium citrate buffer (pH 7.4). The bound silver-gold particles were enhanced using a Silver IntenSE M kit (catalog RPN491; GE Healthcare) for 7 minutes.

Sections were rinsed in 0.1 M PB and then postfixed in 2% osmium tetroxide in PB for 1 hour, dehydrated, and embedded with Epon 812 (Electron Microscopy Sciences) between 2 sheets of Aclar plastic. Sections from dorsal striatum were selected, mounted on EMBed chucks (Electron Microscopy Sciences) and trimmed to 1–1.5 mm–wide trapezoids. Ultrathin sections (~65 nm thick) within 0.1–0.2 μm to the tissue-plastic interface were cut on a Leica Ultracut ultratome, collected into copper mesh grids, and counterstained with uranyl acetate and Reynold's lead citrate. Sections were viewed and photographed using a FEI Tecnai Biotwin electron microscope equipped with a digital camera (Advanced Microscopy Techniques, software version 3.2).

Ultrastructural image analysis. The data analysis procedure is similar as previously described (92). The images were collected at a magnification of 18,500. The dendritic profiles contained regular microtubular arrays and were usually postsynaptic to axon terminal profiles (93). Dendritic spines were small (about 0.1–0.2 μm in diameter), abutted terminals, and sometimes emanated from dendritic shafts (93). Immunoperoxidase labeling for DARPP-32 was distinguished as an electron-dense reaction product precipitate. SIG labeling for NR2A appeared as black electron-dense particles. The criteria for field selection and the measures to avoid false-negative labeling of smaller profiles, variability between animals in each experimental group, and differential reagent sensitivity comparing SIG and immunoperoxidase labeling were performed as described before (91, 93). Profiles were considered dually labeled if they contained immunoperoxidase and at least 1 SIG particle. Fifty dual-labeled dendrites and 50 DARPP-32–labeled dendritic spines from each animal were sampled for electron microscopic analysis.

The subcellular distribution and density of NR2A-SIG particles in Darpp-32–labeled dendrites was determined as previously described (94). For this, the NR2A-SIG particle localization was categorized as (i) on plasma membrane, (ii) near plasma membrane (particles not touching but within 70 nm from the plasma membrane), or (iii) cytoplasmic. The investigator performing the quantification of SIG particles was blinded to the genotypes. MCID imaging analysis software was used to determine the cross-sectional diameter, perimeter, surface area, form factor, and major and minor axis lengths of each immunolabeled dendrite. Only small dendrites (average diameter < 1 μm) were included for analysis. Density of SIG particles is expressed as: (i) number of SIG particles on plasma membrane/perimeter, (ii) number of SIG particles near plasma membrane/perimeter, (iii) number of SIG particles in cytoplasm/area, and (iv) total SIG particles/area.

All DARPP-32–labeled spine profiles that were in contact with axon terminals were further counted and classified as NR2A-labeled (containing at least 1 SIG particle) or non–NR2A-labeled spines. SIG particles in NR2A-labeled spines were additionally classified as cytoplasmic, on/near the plasma membrane (particles within 70 nm from the plasma membrane), or on/near the synapse (particles within 70 nm from the postsynaptic density of the synapse).

Human tissue samples and IHC. Deidentified brain tissue donated from patients with HD (pathological grade 3) and unaffected individuals was obtained from New York Brain Bank at Columbia University. Control tissue was from subjects without HD with similar demographic criteria. Tissues containing caudate and putamen were formalin fixed and paraffin embedded.

IHC was performed using 10 μm–thick sections of formalin-fixed, paraffin-embedded samples. Sections were deparaffinized in xylene and rehydrated in graded alcohols before incubation in phosphate-buffered saline. Slides were then incubated in a steamer in 10 mM citrate buffer (pH 6.0, with 0.05% Tween 20) for 30 minutes to recover antigenic epitopes. Slides were probed with sheep anti–human SorCS2 (R&D Systems, catalog AF4238). Bound antibodies were detected with a biotinylated-conjugated secondary antibody system (Jackson ImmunoResearch Laboratories, catalog 713-065-147) and VIP development according to the manufacturer's protocol (Vector Laboratories, catalog SK-4600). Developed slides were counterstained in hematoxylin (purple stain), dehydrated through graded alcohols, incubated in xylene, and mounted in CytoSeal (Thermo Fisher Scientific). Slide images were captured with an Observer.Z1 (Carl Zeiss), and digital images were acquired with an AxioCam MRc camera and AxioVision 4.8.

Behavioral analyses. All mice were kept on a 12:12 light-dark cycle at 18°C–22°C with food and water available ad libitum unless noted otherwise. All mice for behavioral analyses were brought into the room at least 1 hour before the start of experiment for the purpose of habituation. Only adult male mice (n = 8–12/genotype) were used for behavioral experiments.

Open field. Open field test was used to measure baseline locomotor activity according to previously described procedures (95). Animals were placed in a rectangular open field measuring 21 × 15 inch for 10 minutes. Their activity was recorded by an overhead video camera and analyzed using Ethovision software. Total distance traveled is reported.

Rotarod. Accelerating Rotarod for 5 mice (Panlab/Harvard apparatus) was used to measure motor coordination and balance of mice as described by ref. 96. Animals were trained to stand on a rod rotating at 5 rpm for at least 30 seconds (mice that cannot learn this task were excluded from the experiment). After 1 hour, animals were placed on an accelerating rod that increased in speed from 4 to 40 rpm over the course of a 5-minute trial. Animals were given 5 trials per day for 5 consecutive days. Latency to fall is reported for each trial, and the performance on the last day was used for comparison and statistical analysis.

Inverted lid test. Inverted lid test was described previously to measure muscle strength in mice (97). Mice were placed on a standard cage lid. The lid was gently shaken 3 times, causing the animal to grip the lid. The lid was then quickly inverted and secured 30 cm above a padded surface. Latency to fall was measured, with a maximum trial time of 2 minutes. Each animal was given 3 trials with a 5-minute interval. The maximum of the 3 trials of each animal was used for quantification.

Footprint analysis. For the footprint test, the forepaws and hind paws of the mice were coated with pink and blue nontoxic paints, respectively. The mice were trained to walk along a paper-covered runway that was 50 cm long, 10 cm wide, with 10 cm–high walls into an enclosed box. All the mice were given 3 runs per day for 3 consecutive days. A fresh sheet of white paper was placed on the floor of the runway for each run. The footprint patterns were assessed quantitatively by the measurements of the length of stride and stance, as well as the base width of both forepaws and hind paws.

Statistics. All of the data were analyzed with the program GraphPad Prism version 6.0 (GraphPad Software). Values are presented as the mean ± SEM. When 2 groups were compared, data were analyzed using a nonpaired student's t test. For multiple comparisons, one-way ANOVA followed by Bonferroni post-hoc test was used. Statistical differences were considered to be significant for $P < 0.05$ ($^{*}P < 0.05$, $^{**}P < 0.01$, $^{***}P < 0.001$).

Study approval. All procedures were in accordance with the NIH Guide for the Care and Use of Laboratory Animals and were approved by the Institutional Animal Care and Use Committee of Weill Cornell Medicine. Studies on human brain tissue were approved as being of minimal to no risk or as exempt by the IRBs at Weill Cornell Medicine.

Author contributions

QM performed most of the experiments; SorCS2-KOmice was generated by JY, MEP, and LT; TAM helped carry out the electron microscopy experiments; JGV contributed to the immunostaining analysis performed on the human samples; and BLH, TAM, and QM designed the study and wrote the manuscript.

Acknowledgments

This work was supported by The Cure Huntington's Disease Initiative (CHDI) Foundation (JGV and BLH); National Institute of Health grants NS030687 (BLH), NS064114 (BLH), HL96571 (TAM), HL098351 (TAM), and DA08259 (TAM); Hereditary Disease Foundation (JGV); Hereditary Neurological Disease Centre – Wichita (JGV); Intramural Research Program of National Institute of Health (LT); National Cancer Institute (LT); and the Center for Cancer Research (LT). MEP and LT were supported by the NIH Intramural Research Program, Center for Cancer Research, National Cancer Institute. We thank all members from the BLH laboratory and Carolyn Hill for their assistance. We thank the Neuroanatomy EM Core for use of the facilities. We also express our appreciation to Francis S. Lee for sharing behavioral equipment, discussing the project, and editing the manuscript.

Address correspondence to: Barbara L. Hempstead, Department of Medicine, Weill Cornell Medical College, 1300 York Avenue, New York, New York 10065, USA. Phone: 212.746.2195; E-mail: blhempst@med.cornell.edu.

1. A novel gene containing a trinucleotide repeat that is expanded unstable on Huntington's disease chromosomes. The Huntington's Disease Collaborative Research Group. *Cell*. 1993;72(6):971–983.
2. Roos RA. Huntington's disease: a clinical review. *Orphanet J Rare Dis*. 2010;5:40.
3. Koller WC, Trimble J. The gait abnormality of Huntington's disease. *Neurology*. 1985;35(10):1450–1454.
4. Rao AK, Gordon AM, Marder KS. Coordination of fingertip forces during precision grip in premanifest Huntington's disease. *Mov Disord*. 2011;26(5):862–869.
5. Rao AK, Mazzoni P, Wasserman P, Marder K. Longitudinal Change in Gait and Motor Function in Pre-manifest Huntington's Disease. *PLoS Curr*. 2011;3:RRN1268.
6. Serrien DJ, Burgunder JM, Wiesendanger M. Control of manipulative forces during unimanual and bimanual tasks in patients with Huntington's disease. *Exp Brain Res*. 2002;143(3):328–334.
7. Heindel WC, Butters N, Salmon DP. Impaired learning of a motor skill in patients with Huntington's disease. *Behav Neurosci*. 1988;102(1):141–147.
8. Gabrieli JD, Stebbins GT, Singh J, Willingham DB, Goetz CG. Intact mirror-tracing and impaired rotary-pursuit skill learning in patients with Huntington's disease: evidence for dissociable memory systems in skill learning. *Neuropsychology*. 1997;11(2):272–281.
9. Cattaneo E, Zuccato C, Tartari M. Normal huntingtin function: an alternative approach to Huntington's disease. *Nat Rev Neurosci*. 2005;6(12):919–930.
10. Crook ZR, Housman D. Huntington's disease: can mice lead the way to treatment? *Neuron*. 2011;69(3):423–435.
11. Shoulson I, Chase TN. Huntington's disease. *Annu Rev Med*. 1975;26:419–436.
12. Graybiel AM, Grafton ST. The striatum: where skills and habits meet. *Cold Spring Harb Perspect Biol*. 2015;7(8):a021691.
13. Kemp JM, Powell TP. The structure of the caudate nucleus of the cat: light and electron microscopy. *Philos Trans R Soc Lond, B, Biol Sci*. 1971;262(845):383–401.
14. Vastagh C, et al. N-methyl-D-aspartate (NMDA) receptor composition modulates dendritic spine morphology in striatal medium spiny neurons. *J Biol Chem*. 2012;287(22):18103–18114.
15. Kemp JM, Powell TP. The site of termination of afferent fibres in the caudate nucleus. *Philos Trans R Soc Lond, B, Biol Sci*. 1971;262(845):413–427.
16. Yashiro K, Philpot BD. Regulation of NMDA receptor subunit expression and its implications for LTD, LTP, and metaplasticity. *Neuropharmacology*. 2008;55(7):1081–1094.
17. Dang MT, Yokoi F, Yin HH, Lovinger DM, Wang Y, Li Y. Disrupted motor learning and long-term synaptic plasticity in mice lacking NMDAR1 in the striatum. *Proc Natl Acad Sci USA*. 2006;103(41):15254–15259.
18. Beutler LR, et al. Severely impaired learning and altered neuronal morphology in mice lacking NMDA receptors in medium spiny neurons. *PLoS One*. 2011;6(11):e28168.
19. Dunah AW, Yasuda RP, Luo J, Wang Y, Prybylowski KL, Wolfe BB. Biochemical studies of the structure and function of the N-methyl-D-aspartate subtype of glutamate receptors. *Mol Neurobiol*. 1999;19(2):151–179.
20. Arning L, Kraus PH, Valentin S, Saft C, Andrich J, Epplen JT. NR2A and NR2B receptor gene variations modify age at onset in Huntington disease. *Neurogenetics*. 2005;6(1):25–28.
21. Arning L, Saft C, Wieczorek S, Andrich J, Kraus PH, Epplen JT. NR2A and NR2B receptor gene variations modify age at onset in Huntington disease in a sex-specific manner. *Hum Genet*. 2007;122(2):175–182.
22. Andresen JM, et al. Replication of twelve association studies for Huntington's disease residual age of onset in large Venezuelan kindreds. *J Med Genet*. 2007;44(1):44–50.
23. Young AB, et al. NMDA receptor losses in putamen from patients with Huntington's disease. *Science*. 1988;241(4868):981–983.
24. Dure LS, Young AB, Penney JB. Excitatory amino acid binding sites in the caudate nucleus and frontal cortex of Huntington's disease. *Ann Neurol*. 1991;30(6):785–793.
25. Kent K, Deng Q, McNeill TH. Unilateral skill acquisition induces bilateral NMDA receptor subunit composition shifts in the rat sensorimotor striatum. *Brain Res*. 2013;1517:77–86.
26. Lemay-Clermont J, Robitaille C, Auberson YP, Bureau G, Cyr M. Blockade of NMDA receptors 2A subunit in the dorsal striatum impairs the learning of a complex motor skill. *Behav Neurosci*. 2011;125(5):714–723.

27. Willnow TE, Petersen CM, Nykjaer A. VPS10P-domain receptors - regulators of neuronal viability and function. *Nat Rev Neurosci*. 2008;9(12):899–909.
28. Savas JN, et al. The Sorting Receptor SorCS1 Regulates Trafficking of Neurexin and AMPA Receptors. *Neuron*. 2015;87(4):764–780.
29. Breiderhoff T, et al. Sortilin-related receptor SORCS3 is a postsynaptic modulator of synaptic depression and fear extinction. *PLoS One*. 2013;8(9):e75006.
30. Menalled LB, et al. Comprehensive behavioral and molecular characterization of a new knock-in mouse model of Huntington's disease: zQ175. *PLoS One*. 2012;7(12):e49838.
31. Heikkinen T, et al. Characterization of neurophysiological and behavioral changes, MRI brain volumetry and 1H MRS in zQ175 knock-in mouse model of Huntington's disease. *PLoS One*. 2012;7(12):e50717.
32. Smith GA, et al. Progressive axonal transport and synaptic protein changes correlate with behavioral and neuropathological abnormalities in the heterozygous Q175 KI mouse model of Huntington's disease. *Hum Mol Genet*. 2014;23(17):4510–4527.
33. Plotkin JL, et al. Impaired TrkB receptor signaling underlies corticostriatal dysfunction in Huntington's disease. *Neuron*. 2014;83(1):178–188.
34. Tong X, et al. Astrocyte Kir4.1 ion channel deficits contribute to neuronal dysfunction in Huntington's disease model mice. *Nat Neurosci*. 2014;17(5):694–703.
35. Shirasaki DI, et al. Network organization of the huntingtin proteomic interactome in mammalian brain. *Neuron*. 2012;75(1):41–57.
36. Choy RW, et al. Retromer mediates a discrete route of local membrane delivery to dendrites. *Neuron*. 2014;82(1):55–62.
37. Mangiarini L, et al. Exon 1 of the HD gene with an expanded CAG repeat is sufficient to cause a progressive neurological phenotype in transgenic mice. *Cell*. 1996;87(3):493–506.
38. Gauthier LR, et al. Huntingtin controls neurotrophic support and survival of neurons by enhancing BDNF vesicular transport along microtubules. *Cell*. 2004;118(1):127–138.
39. Marco S, et al. Suppressing aberrant GluN3A expression rescues synaptic and behavioral impairments in Huntington's disease models. *Nat Med*. 2013;19(8):1030–1038.
40. Subramaniam S, Sixt KM, Barrow R, Snyder SH. Rhes, a striatal specific protein, mediates mutant-huntingtin cytotoxicity. *Science*. 2009;324(5932):1327–1330.
41. Zuccato C, et al. Huntingtin interacts with REST/NRSF to modulate the transcription of NRSE-controlled neuronal genes. *Nat Genet*. 2003;35(1):76–83.
42. Sapp E, et al. Huntingtin localization in brains of normal and Huntington's disease patients. *Ann Neurol*. 1997;42(4):604–612.
43. Milnerwood AJ, et al. Early increase in extrasynaptic NMDA receptor signaling and expression contributes to phenotype onset in Huntington's disease mice. *Neuron*. 2010;65(2):178–190.
44. Zeron MM, et al. Increased sensitivity to N-methyl-D-aspartate receptor-mediated excitotoxicity in a mouse model of Huntington's disease. *Neuron*. 2002;33(6):849–860.
45. Zeron MM, et al. Mutant huntingtin enhances excitotoxic cell death. *Mol Cell Neurosci*. 2001;17(1):41–53.
46. Okamoto S, et al. Balance between synaptic versus extrasynaptic NMDA receptor activity influences inclusions and neurotoxicity of mutant huntingtin. *Nat Med*. 2009;15(12):1407–1413.
47. Tang TS, et al. Disturbed Ca2+ signaling and apoptosis of medium spiny neurons in Huntington's disease. *Proc Natl Acad Sci USA*. 2005;102(7):2602–2607.
48. Beal MF, Ferrante RJ, Swartz KJ, Kowall NW. Chronic quinolinic acid lesions in rats closely resemble Huntington's disease. *J Neurosci*. 1991;11(6):1649–1659.
49. Beal MF, Kowall NW, Ellison DW, Mazurek MF, Swartz KJ, Martin JB. Replication of the neurochemical characteristics of Huntington's disease by quinolinic acid. *Nature*. 1986;321(6066):168–171.
50. Graham RK, et al. Differential susceptibility to excitotoxic stress in YAC128 mouse models of Huntington disease between initiation and progression of disease. *J Neurosci*. 2009;29(7):2193–2204.
51. Hansson O, Petersén A, Leist M, Nicotera P, Castilho RF, Brundin P. Transgenic mice expressing a Huntington's disease mutation are resistant to quinolinic acid-induced striatal excitotoxicity. *Proc Natl Acad Sci USA*. 1999;96(15):8727–8732.
52. Sanhueza M, et al. Role of the CaMKII/NMDA receptor complex in the maintenance of synaptic strength. *J Neurosci*. 2011;31(25):9170–9178.
53. Bezprozvanny I. Calcium signaling and neurodegenerative diseases. *Trends Mol Med*. 2009;15(3):89–100.
54. Bezprozvanny I, Hiesinger PR. The synaptic maintenance problem: membrane recycling, Ca2+ homeostasis and late onset degeneration. *Mol Neurodegener*. 2013;8:23.
55. Indersmitten T, Tran CH, Cepeda C, Levine MS. Altered excitatory and inhibitory inputs to striatal medium-sized spiny neurons and cortical pyramidal neurons in the Q175 mouse model of Huntington's disease. *J Neurophysiol*. 2015;113(7):2953–2966.
56. Hardingham GE, Fukunaga Y, Bading H. Extrasynaptic NMDARs oppose synaptic NMDARs by triggering CREB shut-off and cell death pathways. *Nat Neurosci*. 2002;5(5):405–414.
57. Zhou M, Baudry M. Developmental changes in NMDA neurotoxicity reflect developmental changes in subunit composition of NMDA receptors. *J Neurosci*. 2006;26(11):2956–2963.
58. Matteucci A, et al. Curcumin protects against NMDA-induced toxicity: a possible role for NR2A subunit. *Invest Ophthalmol Vis Sci*. 2011;52(2):1070–1077.
59. Guo Z, et al. Striatal neuronal loss correlates with clinical motor impairment in Huntington's disease. *Mov Disord*. 2012;27(11):1379–1386.
60. Aylward EH, et al. Regional atrophy associated with cognitive and motor function in prodromal Huntington disease. *J Huntingtons Dis*. 2013;2(4):477–489.
61. Petralia RS, Al-Hallaq RA, Wenthold RJ. Trafficking and Targeting of NMDA Receptors. In: Van Dongen AM, ed. *Biology of the NMDA Receptor*. Boca Raton (FL): CRC Press/Taylor & Francis; 2009. Chapter 8.
62. Bard L, et al. Dynamic and specific interaction between synaptic NR2-NMDA receptor and PDZ proteins. *Proc Natl Acad Sci USA*. 2010;107(45):19561–19566.

63. Prybylowski K, Chang K, Sans N, Kan L, Vicini S, Wenthold RJ. The synaptic localization of NR2B-containing NMDA receptors is controlled by interactions with PDZ proteins and AP-2. *Neuron*. 2005;47(6):845–857.
64. Lin Y, Jover-Mengual T, Wong J, Bennett MV, Zukin RS. PSD-95 and PKC converge in regulating NMDA receptor trafficking and gating. *Proc Natl Acad Sci USA*. 2006;103(52):19902–19907.
65. Hayashi T, Thomas GM, Huganir RL. Dual palmitoylation of NR2 subunits regulates NMDA receptor trafficking. *Neuron*. 2009;64(2):213–226.
66. Chen ZY, et al. Sortilin controls intracellular sorting of brain-derived neurotrophic factor to the regulated secretory pathway. *J Neurosci*. 2005;25(26):6156–6166.
67. Wang Y, Geng Z, Zhao L, Huang SH, Sheng AL, Chen ZY. GDNF isoform affects intracellular trafficking and secretion of GDNF in neuronal cells. *Brain Res*. 2008;1226:1–7.
68. Andersen OM, et al. Neuronal sorting protein-related receptor sorLA/LR11 regulates processing of the amyloid precursor protein. *Proc Natl Acad Sci USA*. 2005;102(38):13461–13466.
69. Vaegter CB, et al. Sortilin associates with Trk receptors to enhance anterograde transport and neurotrophin signaling. *Nat Neurosci*. 2011;14(1):54–61.
70. Evans SF, et al. Neuronal brain-derived neurotrophic factor is synthesized in excess, with levels regulated by sortilin-mediated trafficking and lysosomal degradation. *J Biol Chem*. 2011;286(34):29556–29567.
71. Xiang J, et al. Huntingtin-associated protein 1 regulates postnatal neurogenesis and neurotrophin receptor sorting. *J Clin Invest*. 2014;124(1):85–98.
72. Gustafsen C, et al. Sortilin and SorLA display distinct roles in processing and trafficking of amyloid precursor protein. *J Neurosci*. 2013;33(1):64–71.
73. Nielsen MS, et al. Sorting by the cytoplasmic domain of the amyloid precursor protein binding receptor SorLA. *Mol Cell Biol*. 2007;27(19):6842–6851.
74. Lane RF, et al. Diabetes-associated SorCS1 regulates Alzheimer's amyloid-beta metabolism: evidence for involvement of SorL1 and the retromer complex. *J Neurosci*. 2010;30(39):13110–13115.
75. Kim E, et al. Implication of mouse Vps26b-Vps29-Vps35 retromer complex in sortilin trafficking. *Biochem Biophys Res Commun*. 2010;403(2):167–171.
76. Fjorback AW, et al. Retromer binds the FANSHY sorting motif in SorLA to regulate amyloid precursor protein sorting and processing. *J Neurosci*. 2012;32(4):1467–1480.
77. Burd C, Cullen PJ. Retromer: a master conductor of endosome sorting. *Cold Spring Harb Perspect Biol*. 2014;6(2):2.
78. Bonifacino JS, Hurley JH. Retromer. *Curr Opin Cell Biol*. 2008;20(4):427–436.
79. Small SA, Petsko GA. Retromer in Alzheimer disease, Parkinson disease and other neurological disorders. *Nat Rev Neurosci*. 2015;16(3):126–132.
80. Steinberg F, et al. A global analysis of SNX27-retromer assembly and cargo specificity reveals a function in glucose and metal ion transport. *Nat Cell Biol*. 2013;15(5):461–471.
81. Muhammad A, et al. Retromer deficiency observed in Alzheimer's disease causes hippocampal dysfunction, neurodegeneration, and Abeta accumulation. *Proc Natl Acad Sci USA*. 2008;105(20):7327–7332.
82. Borgonovo JE, Troncoso M, Lucas JJ, Sosa MA. Mutant huntingtin affects endocytosis in striatal cells by altering the binding of AP-2 to membranes. *Exp Neurol*. 2013;241:75–83.
83. Twelvetrees AE, et al. Delivery of GABAARs to synapses is mediated by HAP1-KIF5 and disrupted by mutant huntingtin. *Neuron*. 2010;65(1):53–65.
84. Rong J, et al. Regulation of intracellular trafficking of huntingtin-associated protein-1 is critical for TrkA protein levels and neurite outgrowth. *J Neurosci*. 2006;26(22):6019–6030.
85. Melone MA, et al. Mutant huntingtin regulates EGF receptor fate in non-neuronal cells lacking wild-type protein. *Biochim Biophys Acta*. 2013;1832(1):105–113.
86. Li X, et al. Mutant huntingtin impairs vesicle formation from recycling endosomes by interfering with Rab11 activity. *Mol Cell Biol*. 2009;29(22):6106–6116.
87. Li X, et al. Aberrant Rab11-dependent trafficking of the neuronal glutamate transporter EAAC1 causes oxidative stress and cell death in Huntington's disease. *J Neurosci*. 2010;30(13):4552–4561.
88. Wu LL, Zhou XF. Huntingtin associated protein 1 and its functions. *Cell Adh Migr*. 2009;3(1):71–76.
89. Li X, et al. Disruption of Rab11 activity in a knock-in mouse model of Huntington's disease. *Neurobiol Dis*. 2009;36(2):374–383.
90. McClory H, et al. Glucose transporter 3 is a rab11-dependent trafficking cargo and its transport to the cell surface is reduced in neurons of CAG140 Huntington's disease mice. *Acta Neuropathol Commun*. 2014;2:179.
91. Milner TA, Waters EM, Robinson DC, Pierce JP. Degenerating processes identified by electron microscopic immunocytochemical methods. *Methods Mol Biol*. 2011;793:23–59.
92. Marques-Lopes J, et al. Female protection from slow-pressor effects of angiotensin II involves prevention of ROS production independent of NMDA receptor trafficking in hypothalamic neurons expressing angiotensin 1A receptors. *Synapse*. 2015;69(3):148–165.
93. Peters A, Palay SL, Webster Hd. *The fine structure of the nervous system: neurons and their supporting cells*. 3rd ed. New York, NY: Oxford University Press; 1991.
94. Van Kempen TA, et al. Alterations in the subcellular distribution of NADPH oxidase p47(phox) in hypothalamic paraventricular neurons following slow-pressor angiotensin II hypertension in female mice with accelerated ovarian failure. *J Comp Neurol*. 2016;524(11):2251–2265.
95. Bath KG, et al. Variant brain-derived neurotrophic factor (Valine66Methionine) polymorphism contributes to developmental and estrous stage-specific expression of anxiety-like behavior in female mice. *Biol Psychiatry*. 2012;72(6):499–504.
96. Shmelkov SV, et al. Slitrk5 deficiency impairs corticostriatal circuitry and leads to obsessive-compulsive-like behaviors in mice. *Nat Med*. 2010;16(5):598–602, 1p following 602.
97. Brooks SP, Dunnett SB. Tests to assess motor phenotype in mice: a user's guide. *Nat Rev Neurosci*. 2009;10(7):519–529.